

AD-A279 279

ED 13-140-10. 1 hour per response, including the time for reviewing instructions, searching existing data sources, obtaining the collection of information, send comments regarding this burden estimate or any other aspect of this item to Washington Headquarters Services, Directorate for Information Operations and Registries, 1215 Jefferson Davis Highway, Washington, DC 20546.

2001/560.11-280.5500

Standard Form 298 (Rev. 2-49)
Amended by AFM 310 / 19-74
AFM 194

THE QUALITY INDEX

OFFICE OF NAVAL RESEARCH

GRANT N00014-92-J-1243

R&T Code 4131065

Scientific Officer: P.P. Schmidt

Technical Report No. 10

**Quantum Simulation of Heterogeneous Electron Transfer Free Energies at the
Water-Metal Interface**

by

Jay B. Straus and Gregory A. Voth

To Be Submitted

to

Journal of Chemical Physics

University of Pennsylvania
Department of Chemistry
Philadelphia, PA 19104-6323

94-14770



May 1994

Reproduction in whole or in part is permitted for any purpose of the United States
Government

This document has been approved for public release and sale; its distribution is
unlimited

94 5 17 001

TECHNICAL REPORT DISTRIBUTION LIST - GENERAL

Office of Naval Research (1)
Chemistry Division, Code 313
800 North Quincy Street
Arlington, Virginia 22217-5000

Dr. Richard W. Drisko (1)
Naval Civil Engineering
Laboratory
Code L52
Port Hueneme, CA 93043

Defense Technical Information
Center (2)
Building 5, Cameron Station
Alexandria, VA 22314

Dr. Harold H. Singerman (1)
Naval Surface Warfare Center
Carderock Division Detachment
Annapolis, MD 21402-1198

Dr. James S. Murday (1)
Chemistry Division, Code 6100
Naval Research Laboratory
Washington, D.C. 20375-5000

Dr. Eugene C. Fischer (1)
Code 2840
Naval Surface Warfare Center
Carderock Division Detachment
Annapolis, MD 21402-1198

Dr. Robert Green, Director (1)
Chemistry Division, Code 385
Naval Air Weapons Center
Weapons Division
China Lake, CA 93555-6001

Dr. Bernard E. Douda (1)
Crane Division
Naval Surface Warfare Center
Crane, Indiana 47522-5000

Dr. Elek Lindner (1)
Naval Command, Control and
Ocean Surveillance Center
RDT&E Division
San Diego, CA 92152-5000

Accession For	
NTIS GRA&I	<input checked="" type="checkbox"/>
DTIC TAB	<input type="checkbox"/>
Unannounced	<input type="checkbox"/>
Justification	
By _____	
Distribution _____	
Availability Codes	
Dist	Avail and/or Special
A-1	

Number of copies to forward

Quantum Simulation of Heterogeneous Electron Transfer Free Energies at the Water-Metal Interface

Jay B. Straus* and Gregory A. Voth

Department of Chemistry, University of Pennsylvania, Philadelphia, PA 19104-6323, USA

Abstract

The free energy for electron transfer is studied for the $\text{Fe}^{2+}/\text{Fe}^{3+}$ charge transfer system at the water-Pt(111) interface. Classical diabatic free energy curves are calculated along with an adiabatic curve based on the Anderson-Newns Hamiltonian. Reactive flux calculations are then performed on this curve to determine the effect of recrossings on the classical rate constant. These effects are not found to be large ($\kappa \sim 0.6$). The solvent model is then extended to a quantum mechanical path integral version and the quantum adiabatic free energy curves are calculated. The resulting quantum effects are found to be quite significant, illustrating that the same electrode overpotential does not necessarily result in the same free energy curves for the classical and quantum mechanical solvent models. These results suggest that classical models for water may not be adequate, or at least need to be modified, for accurate simulations of heterogeneous electron transfer.

Typeset using REVTeX

*Department of Physics, University of Pennsylvania

I. INTRODUCTION

Electron transfer (ET) is a process of fundamental importance in chemistry, physics, and biology [1,2]. The field has seen substantial theoretical research activity, including computer simulations of a variety of homogeneous electron transfer systems, such as charge separation in an ion pair in a polar solvent [3-7] as well as electron transfer in the homogeneous ferrous-ferric system. [8-10] Recently, however, there has been an emerging focus on heterogeneous ET systems [11-13] from the point of view of computer simulation. It is such interfacial charge transfer phenomenon which are important, for example, at a metal electrode immersed in an electrolyte solution. A better understanding of heterogeneous ET processes will be relevant to many areas of technology, ranging from electrochemistry to corrosion to battery technology. The present authors have previously performed simulations examining the free energy curves for a model ion in water near a Pt(111) surface. [11] That work showed an insensitivity of the solvent diabatic free energy curves to surface-induced solvent density inhomogeneities. It also illustrated a substantial adherence to Marcus parabolic behavior [1] over the wide "normal" free energy range, as well as a significant deviation in the inverted regime. The present work significantly extends this area of research with the focus being on a more realistic ferrous-ferric charge transfer system at a platinum electrode. In addition to finding the diabatic free energy curves, a classical adiabatic curve is computed using a model for heterogeneous ET based on the Anderson-Newns Hamiltonian. [14-17] Classical reactive flux calculations are then performed for this system to determine the effect of transition state recrossings within the Marcus theoretical framework for the classical adiabatic rate constant. This latter work is related to the work of Rose and Benjamin except that those authors used a simpler two-state description of the heterogeneous ET Hamiltonian. [13]

In a significant departure from previous simulation studies of heterogeneous ET, a path integral model is developed in order to probe the effects of quantization of the water nuclear motion. This model is employed to determine the quantum adiabatic free energy curves within the context of path integral quantum transition state theory. [18] The important

effects of water quantization on the ET free energies is then assessed, with special attention placed on their magnitude with respect to the size of the classical transition state recrossing effects. It is found that the effect of quantizing the water modes is by far the most important one, leading to the conclusion that the effects of water quantization must be considered in order for simulations of heterogeneous ET to be accurate.

II. METHODS

A. The Anderson-Newns Hamiltonian

Charge transfer between an ion in solution and a metal electrode is represented in the present research by a version [19–21] of an Hamiltonian referred to in the literature as the Anderson-Newns Hamiltonian [14–17]. It can be written as

$$H = H_{\text{solv}} + (\epsilon_a + \Delta E)n_a + \sum_k (\epsilon_k n_k + V_{ak}c_a^\dagger c_k + V_{ka}c_k^\dagger c_a) , \quad (2.1)$$

where H_{solv} represents solvent-solvent, solvent-surface, and all other interactions which do not explicitly involve electronic degrees of freedom, ϵ_a is the vacuum energy level of the acceptor ion's electron orbital which is involved in the charge transfer (orbital "a"), and ΔE is the shift of the energy level due to the presence of the fluctuating solvent. The acceptor orbital has an occupancy n_a equal to either 0 or 1. The sum over k in Eq. (2.1) represents a sum over the electronic energy states ϵ_k in the semi-infinite metal electrode. This summation term clearly includes contributions arising from both the occupancy of the metal electron states as well as a piece which is a "transfer term" giving rise to charge transfer between the states and the ion orbital (c^\dagger and c are creation and annihilation operators respectively).

The Hamiltonian of Eq. (2.1), with its explicit quantum operators, is not yet in a useful form for the purposes of computer simulation. To transform it to the desired form, one can follow the work of Grimley [16] and Muscat and Newns [17]. First, the physically reasonable assumption is made that the solvent adiabatically follows the electronic degrees

of freedom due to the different timescales. One can then examine just the electronic part of the Hamiltonian for a given solvent shift variable ΔE treated adiabatically :

$$H_a = (\epsilon_a + \Delta E)n_a + \sum_k (\epsilon_k n_k + V_{ak}c_a^\dagger c_k + V_{ka}c_k^\dagger c_a) . \quad (2.2)$$

By a series of mathematical manipulations involving the resolvent operator for this Hamiltonian, it can be shown that the ground state electronic energy is given up to a constant by the approximate form [16,17] :

$$E_0(\Delta E) = \frac{\Delta E}{2} + \frac{1}{\pi}(\epsilon_a + \Delta E - \epsilon_f)\tan^{-1}\left(\frac{\epsilon_f - (\epsilon_a + \Delta E)}{\Delta}\right) + \frac{\Delta}{2\pi}\ln\left((\epsilon_a + \Delta E - \epsilon_f)^2 + \Delta^2\right) , \quad (2.3)$$

where ϵ_f is the Fermi level of the metal and Δ is a parameter which measures the broadening of the energy of the orbital a due to the presence of the metal electrons. The parameter Δ is formally given by the expression :

$$\Delta(\epsilon) = \pi \sum_k |V_{ak}|^2 \delta(\epsilon - \epsilon_k) . \quad (2.4)$$

Here, V_{ak} is the matrix element coupling the orbital and a particular metal electron state k . As it is roughly insensitive to the energy ϵ for energies in the range of interest, Δ is typically taken as a constant.

The net effect of the preceding manipulations is that *classical* dynamics can now be run on the Hamiltonian $H_{\text{solv}} + E_0(\Delta E)$ which represents the adiabatic ground state behavior of the Hamiltonian of Eq. (2.1). This result is obtained because one can easily assign ΔE to certain classical potential energies in a typical molecular dynamics simulation. In particular, in the Hamiltonian for the present simulation one can separate out all the terms that depend on the Coulombic interaction between the solvent and the ion. One can then write those terms in a form assuming a ferric ion (Fe^{3+}) with a positive charge Z ($Z = 3$) which has an electron orbital of occupancy n_a . If the orbital is empty, then $n_a = 0$, and the Hamiltonian effectively reduces to that describing the Fe^{3+} ion solvated near the metal surface. If the ion orbital is filled, however, then $n_a = 1$ and the Hamiltonian describes the combination

of the Fe^{3+} ion with the negatively charged electron, i.e., a solvated ferrous ion (Fe^{2+}) near the surface. The overall Coloumbic terms are thus given by :

$$(Z - n_a)(V_{s,ion} - V_{s,image}) \quad (2.5)$$

Here, $V_{s,ion}$ indicates the potential energy between the solvent and a single positive charge at the ion's position, while $V_{s,image}$ indicates the potential energy between the solvent and a unit negative charge at the position of the ion's image. In order to make a correspondence between Eq. (2.5) and the Anderson-Newns Hamiltonian of Eq. (2.1) one must therefore specify

$$\Delta E = -(V_{s,ion} - V_{s,image}) \quad (2.6)$$

The Z -dependent terms in Eq. (2.5) are grouped with the rest of the interactions in the solvent Hamiltonian H_{solv} .

The end result of the analysis is that adiabatic computer simulations can be performed for an Fe^{3+} ion and its image, with an additional term in the Hamiltonian representing the electronic degrees of freedom given by Eq. (2.3). One therefore expects the free energy curves will display the approximate form [21,19,20] :

$$F(\Delta e) = \frac{1}{4\lambda}(\Delta E - \Delta E_{min})^2 + E_0(\Delta E) \quad (2.7)$$

Here, λ is the reorganization free energy obtained from a best fit parabola to the diabatic Fe^{3+} free energy curve, and ΔE_{min} gives the location of the minimum of the diabatic curve.

Standard umbrella sampling techniques (see, e.g., refs. [5,8] can be applied to calculate the adiabatic free energy curve as a function of ΔE and find the free energy barrier to the charge transfer reaction involving the ionic orbital a . Also, the average occupancy of the acceptor orbital a at any point along the free energy curve can be shown to be given by [16,17]

$$\langle n_a(\Delta E) \rangle = 1/2 + (1/\pi)\tan^{-1} \left(\frac{\epsilon_f - (\epsilon_a + \Delta E)}{\Delta} \right) \quad (2.8)$$

Equation (2.8) serves as a useful summary of the behavior of the Anderson-Newns Hamiltonian. The average occupancy of the orbital a on the ion, $\langle n_a(\Delta E) \rangle$, smoothly goes from 0 to 1 as a function of the shift in its energy due to the solvent, given by ΔE . If the solvent shift takes on a value such that the energy level is altered to coincide with the Fermi level of the metal, the average occupancy is one-half (i.e., the electron transfers). The parameter Δ measures how quickly the transition from 0 to 1 occurs as ΔE is varied, which is in keeping with its role as an energy level broadening.

B. Model

Some of the simulation details in the present work were presented in an earlier article by the present authors [11] but are repeated again here in the interest of completeness. The solvent consisted of 671 water molecules described by a flexible SPC model [22,23]. This model was modified in a fashion which is inconsequential for the classical case, but is important for later generalization to the quantum case, and is discussed in Appendix A. A temperature of 300 K was maintained during the simulation by using one Nosé thermostat [24] on the oxygens, and another on the hydrogens.

The water molecules in the simulation were situated at the interface with a Pt(111) electrode surface. The interactions between the water molecules and the platinum surface were given by the potential developed by Raghavan et al. [25] which, in turn, was developed by fitting to the water-platinum atom potential given by Spohr and Heinzinger [26]. Since this effective potential represents the Pt(111) plane with its fcc lattice structure, the potential exhibits an hexagonal symmetry. Moreover, this potential represents the corrugated Pt (111) surface without including individual platinum atoms in the simulation. Using such an effective potential is advantageous as one does not have to devote significant computer resources to the integration of the metal atoms' trajectories which are unlikely to contribute significant effects.

Hexagonal periodic boundary conditions were not employed in the present study as in

the study of Raghavan et al. [25] Rather, a carefully chosen rectangular cell was employed whose sides of length $3s$ and $\sqrt{3}s$ can inscribe a hexagon of side length s , shown in Fig. 1. Periodicity was enforced in the x and y directions. Such a simulation cell can accommodate the underlying hexagonal symmetry of the (111) surface, as shown in Fig. 2. For the particular case of the (111) face of platinum, the smallest hexagon that could be formed had a side of length 2.77 Å. A central hexagon with a side five times larger, or 13.86 Å, was chosen which gave a box length in the z direction of 41.6 Å and in the y direction of 24.0 Å. The water-water interactions were smoothly cut-off by half the y box length, going to zero at 12.0 Å. The smooth cut-off began at a distance of 10.3 Å.

While the bottom of the periodic cell was bounded by the platinum surface, the top of the cell was bounded by a featureless slab. The parameters for the interaction of this slab with a water molecule were taken from the “soft” water-metal potential of Hautman, Halley, and Rhee [28], with the image terms omitted. The height of this slab was adjusted to give bulk water density in the middle 5 Å of our cell, giving the periodic cell a length in the z direction of 22.5 Å.

Raghavan et al. [25] have demonstrated that their potential leads to a rather interesting water structure at the metal liquid interface for SPC/E water [29]. Since the distance between the platinum atoms on the (111) face (~ 2.77 Å) is commensurate with the distance between water molecules in ice, the waters apparently form an ice-like layer on top of the Pt(111) face which exhibits hexagonal ordering even at room temperature. There is also a second layer of waters which is hydrogen bonded to the first one. Beyond the second layer, however, the water exhibits essentially bulk-like characteristics (although there is some hint of a moderate nonuniformity in density which could be interpreted as corresponding to a third partially ordered layer). It should be noted that even though a flexible water model has been employed in the present study which is slightly different from rigid SPC/E, it was again verified that the water interaction with the platinum surface again gives rise to a similar water double layer structure.

The iron ion was fixed 5.1 Å above the center of the platinum surface which places it in

the center of the second layer of waters. This placement is in accordance with the work of Rose and Benjamin [13]. The interaction between the iron and the water was taken from Kuharski et al. [8]. It essentially consists of a Coloumbic interaction between the charge on the ion with the partial charges on the SPC water, along with a repulsive potential between the iron and the oxygens. In addition to this iron ion, an image charge of the ion was introduced below the surface, as discussed in Appendix B. All iron-water interactions were cut-off in the same fashion as were the water-water interactions.

C. Free Energy Sampling Method - Umbrella Sampling

The free energy curve $F(\Delta e)$, is related to the probability of observing a certain value of the energy gap function $\Delta E = \Delta e$. Therefore one could run simulations in equilibrium and via some sort of binning arrangement calculate the probability of obtaining various values of Δe and thereby extract $F(\Delta e)$. However the reactive ET event occurs very infrequently. Consequently one would be unable to effectively sample these important transitional regions of the free energy curve using a realistic amount of computer time. The solution to this problem is to add a biasing potential to force the system to obtain a particular range of values of Δe and then remove the effect of the potential when calculating $F(\Delta e)$. One can see how to do this by simply rewriting the equilibrium average of some quantity A in the system described by a Hamiltonian H (i.e. $\langle A \rangle_H$) in terms of a different system with the added biasing potential V_b :

$$\langle A \rangle_H = \frac{\int dx e^{-\beta H} A}{\int dx e^{-\beta H}} = \frac{\int dx e^{-\beta(H+V_b)} e^{\beta V_b} A}{\int dx e^{-\beta H}} \times \frac{\int dx e^{-\beta(H+V_b)}}{\int dx e^{-\beta(H+V_b)}} \quad (2.9)$$

$$\langle A \rangle_H = \langle A e^{\beta V_b} \rangle_{H+V_b} \langle e^{-\beta V_b} \rangle_H \quad (2.10)$$

Specializing to the case $A = \delta(\Delta e - \Delta E)$ and $V_b = V_b(\Delta E)$, and using the definition of the free energy (up to an overall constant), one obtains

$$F(\Delta e) \equiv -k_B T \ln \langle \delta(\Delta e - \Delta E) \rangle_H \quad (2.11)$$

$$= -k_B T \ln \langle \delta(\Delta e - \Delta E) \rangle_{H+V_b} - V_b(\Delta e) + c . \quad (2.12)$$

Here c is some constant that depends on the specific choice of the biasing potential V_b . By using a series of biasing potentials in overlapping regions of the variable Δe , i.e. "windows", one can match up the results and form a smooth curve of $F(\Delta e)$ for the original system, even in otherwise infrequently sampled regions relevant to the ET process. [5,8]

D. Reactive Flux Calculations

In the adiabatic limit, the Marcus rate constant is essentially a classical transition state theory expression obtained by using Δe as the reaction coordinate. [1] In other words, the theory ignores dynamical recrossings so that once the reaction coordinate passes through the transition state towards the product it is assumed that it will never turn around and come back. A standard technique known as the reactive flux correlation function [30] has been developed to efficiently calculate the effect of these recrossings - an effect which is expressed in terms of a prefactor κ to the TST rate constant. The reactive flux correlation function expression for κ has its origin in the classical expression for the rate constant to go from a stable state A (reactant) to a stable state B (product) :

$$k_{BA} = (x_A)^{-1} \langle \dot{q}(0) \delta(q(0) - q^*) \theta_B(q(t)) \rangle . \quad (2.13)$$

Here, q is the generalized reaction coordinate, q^* denotes its transition state value, θ_B is a unit step function with its origin at the transition state, and x_A denotes the molar fraction in the reactant state ($x_A + x_B = 1$). The zero time limit of this expression gives the TST rate constant [30] which assumes no recrossings and is an upper bound to k_{BA} :

$$k_{TST} = (x_A)^{-1} \langle \dot{q}(0) \delta(q(0) - q^*) \theta_B(\dot{q}(0)) \rangle . \quad (2.14)$$

Since the TST quantity is an upper bound, one can write the exact rate constant as

$$k_{BA} = \kappa k_{TST} , \quad (2.15)$$

where $\kappa \leq 1$. The closer κ is to unity the less important are the transition state recrossings. With $\langle \dots \rangle_s$ denoting here the constraint $q = q^*$ for the initial conditions, one can write

$$\kappa = \frac{\langle \dot{q}(0)\theta_B(q(t)) \rangle_{\delta}}{\langle \dot{q}(0)\theta_B(\dot{q}(0)) \rangle_{\delta}} \quad (2.16)$$

which can be broken up into initially positive and negative trajectories, i.e.,

$$\kappa = \frac{\langle \dot{q}_+(0)\theta_B(q(t)) \rangle_{\delta}}{\langle \dot{q}_+(0) \rangle_{\delta}} + \frac{\langle \dot{q}_-(0)\theta_B(q(t)) \rangle_{\delta}}{\langle \dot{q}_-(0) \rangle_{\delta}}. \quad (2.17)$$

Usually, one can switch to a flux-weighted distribution [30] to obtain better sampling of the relevant initial conditions. In this case, the transmission coefficient is given by

$$\kappa = \frac{1}{N_+} \sum_{j=1}^{N_+} \theta_B(q_j^+(t)) - \frac{1}{N_-} \sum_{j=1}^{N_-} \theta_B(q_j^-(t)), \quad (2.18)$$

where the trajectories are implicitly sampled from the flux-weighted distribution function. The quantity κ is taken from the simulation during a period of time in which it is essentially time-independent and achieves its “plateau value”. [30,31]

In the present study, a modification of the foregoing expressions was necessary. For the reaction coordinate under consideration, ΔE , the implementation of a flux-weighted distribution is not straightforward. This is because it is difficult to constrain ΔE while leaving $\Delta \dot{E}$ unconstrained in a simple way. Instead one can use the expression

$$\kappa = \frac{\langle \langle \Delta \dot{E}(0)\theta(\Delta E(t) - \Delta e^*) \rangle_{\dot{q}} \rangle_{q,\delta}}{\langle \langle \Delta \dot{E}(0)\theta(\Delta \dot{E}(0)) \rangle_{\dot{q}} \rangle_{q,\delta}}, \quad (2.19)$$

where $\langle \dots \rangle_{\dot{q}}$ indicates an average over the velocity distribution, and $\langle \dots \rangle_{q,\delta}$ indicates an average over the spatial terms with an implicit δ function fixing the reaction coordinate at the transition state.

III. RESULTS

A. Diabatic Free Energy Curves

An important ingredient for formulating the Anderson-Newns model for heterogeneous ET is the diabatic Marcus free energy curves. Therefore, simulations were first performed for an ion of fixed charge and with no additional term representing the electronic degrees of

freedom. The free energy as a function of the solvent coordinate is defined up to a constant by setting the probability of finding a certain value Δe of ΔE as equal to $\exp[-\beta F(\Delta e)]$. More explicitly, one has [5,4]:

$$F(\Delta e) = -k_B T \ln \left[\int dx \delta(\Delta E(x) - \Delta e) e^{-\beta V(x)} \right] , \quad (3.1)$$

where x represents the multidimensional coordinates of the entire system.

Analogous to the discussion in our earlier paper [11], the reaction coordinate can be written as the negative of the difference of the solvent interacting with the $3+$ ion and the $2+$ ion, since the non-coulombic interactions are identical in both cases. Using this fact and Eq. (3.1), it can be shown [4] that the free energy curves satisfy :

$$F_{2+}(\Delta e) = F_{3+}(\Delta e) + \Delta e \quad (3.2)$$

As a result of the above argument, only the $2+$ diabatic free energy curve was calculated by the techniques of umbrella sampling [5,8], and the $3+$ curve was generated via Eq. (3.2). Parabolic biasing potentials on the solvent coordinate $\Delta E(x)$ were used to define the umbrella sampling windows, and each window was first equilibrated for over 10 picoseconds. Then the data were collected for each window from 8 ps trajectories. A total of 62 partially overlapping windows were employed to generate the curves shown in Figure 3.

Before computing the adiabatic free energy curves, one needs to use the diabatic curves to find the reorganization energy λ and the location of the minimum of the Fe^{3+} curve, Δe_{\min} . It has been shown by Schmickler [19] that if the diabatic free energy curves are parabolic the adiabatic free energy curves will have the form of a symmetric double well provided the overpotential η is set to zero. The latter quantity is defined by

$$\eta \equiv \epsilon_a - \epsilon_f + \Delta e_{\min} - \lambda . \quad (3.3)$$

The quantity $\epsilon_a - \epsilon_f$ is adjustable by simply varying the external potential of the electrode, but one must know the other quantities in the above expression in order to affect the desired adjustment to achieve the desired symmetric form. Assuming parabolic behavior, the $3+$

curve should satisfy the equation $y = 1/4\lambda(\Delta e - \Delta e_{\min})^2 + c$, and a least squares fit to the classical data in Figure 3 gives $\lambda = 57.3$ kcals and $\Delta e_{\min} = 449.7$ kcals, each correct to about 0.5 kcals. Thus, there will be an error of approximately 0.7 kcal in the effort to achieve a zero overpotential.

B. Adiabatic Curves

For a given overpotential (e.g. zero in the present case), one can determine the adiabatic curves using the Anderson-Newns Hamiltonian (i.e., with Eq. (2.3) included in the dynamics) and umbrella sampling. Following the same techniques as described previously, the adiabatic curve was found for $\Delta = 0.05$ e.v. as shown in Figure 4. Twenty eight partially overlapping sampling windows were used to compute the curve. Once the adiabatic curve was calculated, the top of the barrier was found to be at $\Delta e^* = 390.5$ kcals ± 0.5 kcals. By using this information, reactive flux techniques could then be used to determine the importance of dynamical recrossing effects in the ET rate constant. [13]

C. Recrossing Behavior

As discussed earlier, the effects of classical recrossings of the transition state are measured by a quantity κ given by Eq. (2.19). In that equation, Δe^* indicates the transition state value of ΔE and the symbol $\langle \dots \rangle_q$ denotes an equilibrium average over all the individual solvent momenta. The symbol $\langle \dots \rangle_{q,\delta}$ denotes an equilibrium average over all the individual solvent coordinates with the multidimensional reaction coordinate ΔE constrained by a δ function to be at Δe^* . In practice this quantity was determined by running trajectories held in the area of the barrier top by a constraining potential which is a function of ΔE . When ΔE passed through the barrier top, that solvent coordinate configuration was saved and the solvent momenta were reselected from the appropriate Boltzmann distribution. A number of such trajectories with reselected momenta were then run and the nested averaging was performed over these trajectories with different momenta (the Nosé thermostats were turned

off for this procedure). More runs were then performed for different solvent configurations at the barrier top, so as to arrive at a final converged value of κ .

Owing to the discrete timestep in the simulations, the values of ΔE which were saved were very slightly off the exact chosen barrier, whether to the right or the left. The net effect of this numerical uncertainty is that a delta function constraint is not precisely enforced for the reaction coordinate at the top of the barrier. (This is allowed in the reactive flux method provided the barrier is high and the stable states are well separated. [30]) One can then deduce from Eq. (2.19) that the zero time value of κ will be ≈ 0 , but it rises quickly and subsequently falls off to the final plateau value. The graph of κ versus time is shown by Fig. 5 for the present system. In the calculations, 112 different starting configurations of the solvent were used to generate the graph, each one being run with 100 reselected momenta configurations. The final value for κ is $0.5769 +/ - 0.0004$. This shows that recrossing effects do not substantially cast a shadow on the TST (Marcus) estimate of the ET rate constant which describes the rate over many orders of magnitude.

IV. QUANTUM EFFECTS

A. Path Integral Methods

Since classical recrossings are found to have little effect on the overall rate constant, the role of quantum mechanical solvent effects was next examined. An earlier study of the homogeneous $\text{Fe}^{2+}/\text{Fe}^{3+}$ ET system found tunneling of the water librational modes can have a substantial impact on the rate constant, [9] although it has been suggested [10] that the latter effect may be somewhat enhanced by the particular model used for water. Clearly, the issue of solvent quantization is an important one in ET theory, and the present study examines these effects for the first time for the quite different case of heterogeneous ET.

The quantum mechanical simulations were carried out using the well-established technique of path integral molecular dynamics [32,33]. In order to use such a simulation to

actually calculate an activated rate constant, path integral quantum TST was used. [18] This theory provides a quantum mechanical analogue for the classical TST activation free energy by expressing the quantum rate constant k as

$$k = \kappa k_{QTST} \quad (4.1)$$

where κ is a quantum correction factor of order unity (but not necessarily less than unity), and k_{QTST} can be written in the approximate form

$$k_{QTST} \approx \frac{\omega_0}{2\pi} e^{-\beta\Delta F_c^*}$$

Here, ΔF_c^* is the difference in free energy from the well to the barrier of the quantum free energy curve corresponding to the path centroid of the reaction coordinate ΔE . In the present case, the reaction coordinate centroid is defined as

$$\Delta E_0 = \frac{1}{\hbar\beta} \int_0^{\hbar\beta} d\tau \Delta E(\tau) = \frac{1}{P} \sum_{i=1}^P \Delta E(x_i) \quad (4.3)$$

The quantity ω_0 in Eq. (4.2) is the frequency of the reactant well corresponding to the centroid thermal motion in that region. The transition state configuration in the path integral QTST is given by $\Delta E_0 = \Delta e_c^*$, i.e., the maximum of the quantum free energy curve. The adiabatic free energy curves of the centroid of $\Delta E(\tau)$ will therefore be the subject of interest in the following discussion. The notation Δe_c will be used to refer to a particular value of the centroid ΔE_0 when discussing the quantum simulation; the context of the usage should remove any potential confusion with the classical case.

In path integral simulations, the isomorphic quasiparticle polymer which represents a quantum particle [33] is spread out in space, but collapses towards a point particle, and becomes more classical-like, in the limit of high temperature or large mass. As a consequence, only the hydrogens of the water model were discretized; the oxygens are over an order of magnitude more massive and were treated classically.

The mass of the quasiparticles in the discretized path integral is an arbitrary parameter. In practice, however, during molecular dynamics simulations one would prefer larger velocities so that the hydrogen polymers more evenly sample the available phase space. This

can be accomplished by choosing smaller quasiparticle masses, but masses too small give velocities so large that they pose difficulties for the numerical integrator and lead to non-ergodic sampling. A mass of 50 a.u. was found to be suitable on both fronts. In addition, one needs to select a value of the discretization parameter P (i.e., the number of quasiparticles). [18] Ideally, the value of P selected would be the smallest one which exhibits the proper convergence in the interest of computation effort. In order to estimate the value of P which gives such convergence, a Monte Carlo study was performed by Lobaugh [34]. This study was along the lines of one suggested by Kuharski and Rossky [35]. It consisted of two solvent water molecules which interacted using the flexible SPC potential and an additional quadratic constraining potential between their centers of mass. This potential had a minimum at 2.85 Å and a frequency $\omega = 26 \text{ ps}^{-1}$, creating an environment similar to the bulk solvent. A total of 10^6 trial Monte Carlo moves were carried out and a number of different properties were examined as a function of P , including radial distribution functions and the bond length average $\langle r_{OH} \rangle$. The value $P = 25$ was selected as exhibiting sufficient convergence in these properties; for example, a graph of $\langle r_{OH} \rangle$ vs. P is shown in Fig. 6.

The application of the path integral discretization scheme to a classical model for water involves the assumption that the classically optimized water model will still provide a good representation for actual water in the quantum limit. One drawback of this approach is that the parameters of the water model were developed classically to model actual water. Fortunately, at room temperature, the classically accessible regions provide the dominant contribution to the physical properties. Technically, however, the model should be reparameterized in the quantum limit. Another drawback, which has also not yet been fully investigated due to the computational cost, is that the quantum version of the water may explore regions of the potential energy surface that are classically inaccessible. Thus, the functional form of the potential in these regions may not be correctly parameterized to reproduce the physical properties of water. For example, it was found that the discretized version of the classical model dissociates at infrequent intervals as the potential is not bounded along the O-H bonds. This resulted from occasional unphysical tunneling of an hydrogen to another

nearby water molecule (roughly 1 dissociation occurred for every 500 water molecules in a picosecond of simulation). To prevent this behavior from occurring, the potential was modified by the addition of a hard repulsive wall along the O-H bond. As discussed in Appendix A, this wall was adjusted to prevent the dissociations without affecting the thermodynamic properties of either the quantum or classical versions of the water.

The numerical techniques used for the quantum case were essentially identical to the classical case. Again two Nosé thermostats were used; one on the oxygens and one on all of the hydrogen quasiparticles. The solvent coordinate consists of the same Coulombic interactions, with the exception that each hydrogen quasiparticle acts to create a potential at the ion site as would a charge of magnitude $+1/P$. The same value of $\epsilon_a - \epsilon_f$ was used in order to fairly compare the quantum adiabatic curves with the classical ones (i.e. to be able to clearly discern quantum solvent effects for a single underlying Hamiltonian).

B. Quantum Results

The results from the quantum umbrella sampling, which contains contributions from 9 sampling windows, are shown in Fig. 7. It should be noted that with $P = 25$ the simulation requires roughly 11 times more computer time than the classical case to complete a given run. In fact, the present simulation seems to be the most ambitious simulation of quantized water attempted to date. All modes of the flexible model have been quantized and a relatively large number of water molecules were used (671). The simulation required the dedicated use of five high end computer workstations (e.g. HP/Apollo 735) for 4 months along with 200 CPU hours on a Cray C90. Of course, in the future such computations will become more commonplace as computers increase in speed.

As can be seen in Fig. 7, the quantization of the solvent model has a significant effect on the free energy curves. The same value for $\epsilon_f - \epsilon_a$ was used as in the classical case, but now the curves are no longer symmetric. The overpotential in the quantum case is 10.3 kcals, creating free energy curves which are in marked contrast to the symmetric classical case. This

behavior results because the minimum reaction coordinate value is shifted from 449.7 kcals to 464.3 kcals in the quantum case, while λ has shifted from 57.3 kcals to 61.6 kcals. The quantum barrier height from the $\sim 2+$ well is 8.9 kcals, as opposed to 11.2 kcals in the classical case. For the $\sim 3+$ well, the quantum barrier is 19.1 kcals as opposed to the classical 12.7 kcals. The results illustrate that the same electrode overpotential will not necessarily result in similar adiabatic free energy curves in the classical and quantum mechanical models. In fact, the thermodynamic driving force is substantially different for the two cases, reflecting the differences in solvation of the ion by the classical and quantum water models. These differences in free energies would have quite large effects on the rates. This study therefore strongly suggests the importance of treating quantum solvent effects within the quantum TST expression (i.e. a factor of 60 for the oxidation of Fe^{2+} and of 4×10^4 for the reduction of Fe^{3+}) in studies of heterogeneous electron transfer rates for aqueous solutions.

V. CONCLUDING REMARKS

The present studies have examined the role of both a classical and quantum mechanical water solvent model with regards to electron transfer across the water-metal interface. Within a Marcus theory framework, solvent dynamical effects have been shown to be of relatively minor importance. A comparison of the quantum adiabatic free energy curves with the corresponding classical curves has shown, on the other hand, a considerable impact from quantum effects. Since a quantum solvent model more accurately describes the actual physical system, this result suggests that a classical simulation may not be adequate for the study of heterogeneous ET.

A comparison of the present results with those of Bader et al. [9] on the quantum solvent effects in the homogeneous $\text{Fe}^{2+}/\text{Fe}^{3+}$ ET system is in order. In the latter study, the path integral method was used to quantize the rigid SPC model for water. In that case, the important librational motions of the water dipoles were quantized and therefore allowed to tunnel in the symmetric $\text{Fe}^{2+}/\text{Fe}^{3+}$ ET process. Indeed, these librational tunneling effects

were estimated to be significant (a factor of 60), although Song and Marcus [10] suggest this factor would be revised downward by considering a more realistic solvent spectral density. In the present simulations of the single ion, heterogeneous ET process, all of the modes of the flexible SPC model have been quantized. Therefore it is more difficult to specifically attribute the quantum effects to librational tunneling (although they are surely present). Moreover, the heterogeneous $\text{Fe}^{2+}/\text{Fe}^{3+}$ ET system is quite different from the homogeneous case, since the symmetry of the homogeneous system is broken by replacing one of the iron ions with a metal electrode. In the heterogeneous case, the differences in the classical versus quantum ion solvation may be the dominant effect which, in fact, leads to changes in the thermodynamic driving force for the reaction (c.f. Fig. 7). Such effects are not possible in the symmetric homogeneous $\text{Fe}^{2+}/\text{Fe}^{3+}$ ET system.

Future research must include a thorough and costly examination of the quantum water model to insure its accuracy. It is unclear whether the relatively straightforward extension of a classical model to the quantum regime via a path integral discretization scheme provides a sufficiently accurate representation of physical water without reparameterization of the model. Of particular concern are the regions of the potential which are classically inaccessible. Such regions will undoubtedly need at least minor modification. Additional research must also include an examination of the role of solvent electronic polarizability, as well as a serious attempt to develop an effective classical water model which can capture the quantum solvation effects. [36] The important issues of the water/surface interaction and the electronic exchange term Δ (c.f. Eq. 2.4) clearly require some serious theoretical attention, as does the problem of finite ion concentrations. These and other issues will surely make the theoretical study and simulation of heterogeneous ET processes a challenging and stimulating endeavor.

ACKNOWLEDGMENTS

This research was supported by the Office of Naval Research. G.A.V. is a recipient of a National Science Foundation Presidential Young Investigator Award, a David and Lucile Packard Fellowship in Science and Engineering, an Alfred P. Sloan Foundation Research Fellowship, and a Dreyfus Foundation New Faculty Award. The authors acknowledge grant numbers CHE920053P and MCA94P017P at the NSF Pittsburgh Supercomputing Center. The authors also acknowledge the assistance of John Lobaugh in developing the path integral water solvent model.

APPENDIX A: THE HARD WALL MODIFICATION TO THE FLEXIBLE SPC WATER MODEL IN THE QUANTUM LIMIT

In this Appendix, a hard wall modification to the flexible SPC water model is presented. As discussed earlier, it was found that the discretized path integral version of the flexible SPC water model dissociates at infrequent intervals since the potential is not bounded along the O-H bonds. This behavior results from occasional unphysical tunneling of an hydrogen from a water molecule to an oxygen site on a nearby water molecule. To prevent this situation from occurring, the potential was modified by the addition of a hard repulsive wall along the O-H bond, given by the functional form

$$V_{\text{wall}} = \frac{a_h}{(r_{OH_1} - r_h)^{12}} + \frac{a_h}{(r_{OH_2} - r_h)^{12}} , \quad (A1)$$

where $a_h = 15.13 \text{ (kcal/mole)}(\text{\AA})^{12}$ and $r_h = 2.6 r_{OH,\text{eq}}$, where $r_{OH,\text{eq}}$ is the equilibrium OH bond length distance. These parameters were adjusted to prevent the dissociations without affecting the thermodynamic properties of either the quantum or classical versions of the water.

Several test simulations were carried out with $P = 5$ in a three dimensional periodic cube with 512 water molecules. It was found that for $r_h = 2.8 r_{OH,\text{eq}}$, or larger, the waters still dissociated. As tunneling effects will surely increase with larger P , this behavior will

clearly be present for $P = 25$. For a value of $r_h = 2.6 r_{OH,eq}$ the dissociations ceased. It was also explicitly verified that this value of r_h prevents the dissociations with $P = 25$ and does not affect the known properties of SPC water. In addition, the average total intramolecular potential for the $P = 5$ case was examined as a function of r_h and was found to have converged by $r_h = 2.6 r_{OH,eq}$. This behavior is shown in Fig. 8.

APPENDIX B: IMAGES AT THE DIELECTRIC-CONDUCTOR INTERFACE IN COMPUTER SIMULATIONS

In this Appendix, the incorporation of image charges into molecular dynamics simulations at a dielectric-conductor interface is examined. This analysis is performed in such a way as to make the appropriate connections with a dielectric continuum model and a perfectly flat conducting surface.

If an ion is in solution near a conducting surface, one would expect an image term to be present in the Hamiltonian for the system. In fact, it is a classic problem to have a charge q imbedded in a dielectric medium of dielectric constant ϵ_1 , near the interface with another medium of dielectric constant ϵ_2 (the conducting case corresponds to the limit of $\epsilon_2 \rightarrow \infty$). If the half space $z > 0$ is filled with dielectric ϵ_1 , while $z < 0$ is filled with dielectric ϵ_2 , Jackson [37] solves for the potential Φ when a charge q is imbedded in medium 1 a distance d from the interface. For the region $z > 0$ the solution is :

$$\Phi = \frac{q}{\epsilon_1 R} + \frac{q'}{\epsilon_1 R'} , \quad (B1)$$

where R measures the distance from an observer to the charge q , and R' measures the distance from an observer to an image charge q' which is located a distance d behind the interface (and thus $2d$ from the actual charge q). The image charge has a magnitude given by :

$$q' = -\frac{\epsilon_2 - \epsilon_1}{\epsilon_2 + \epsilon_1} q . \quad (B2)$$

One possible interpretation for the potential given in Eq. (B1) is to regard the expression as representing two actual charges q and q' imbedded in a medium of dielectric constant ϵ_1 which fills *all* of space, keeping in mind that one can only use the equation for the $z > 0$ region. In the $z < 0$ region the potential is given by

$$\Phi = \frac{1}{\epsilon_2} \frac{q''}{R} , \quad (B3)$$

where R measures the distance from the actual charge q , and q'' is given by

$$q'' = \frac{2\epsilon_2}{\epsilon_2 + \epsilon_1} q \quad (B4)$$

For the case under study in the present work, medium 2 is a conductor, so one is interested in the field in the $z > 0$ region when $\epsilon_2 \rightarrow \infty$. Equation (B2) clearly shows that $q' = -q$, and the potential from Eq. (B1) gives :

$$\Phi_{\text{solvent}} = \frac{q}{\epsilon_1 R} + \frac{-q}{\epsilon_1 R'} . \quad (B5)$$

While Eq. (B5) is the correct expression for the field in dielectric 1, it is nevertheless not yet in a form useful for direct incorporation into a molecular dynamics simulation. The reason for this lies in the manner in which such a simulation takes into account the dielectric constant. No explicit dielectric constant is ever introduced into the intermolecular forces. Rather the intermolecular forces allow for an orientational polarizability (or other forms of polarizability as well, depending on the model) which responds to an applied electric field in such a manner as to behave as a dielectric of constant ϵ_1 . For SPC water at standard temperature and pressure ϵ_1 has been computed to be $65 +/ - 9$ [8] while the experimental water value is 80. It is seen that even though the expression for the potential from a charge in bulk dielectric may be $q/\epsilon_1 R$, we would carry out this simulation on a computer by simply allowing the solvent to relax around the charge without any direct introduction of ϵ_1 ; a properly constructed solvent model will already take into account its dielectric nature. It will arise of its own accord. Correspondingly, if one wished to carry out a simulation which would give the potential shown in Eq. (B5), one cannot simply introduce an image charge

and an explicit dielectric constant. Rather, we would have to do a bulk simulation where the solvent is extended to the $z < 0$ region and surrounds a charge q' . This is undesirable for several reasons. First of all, it eliminates not only the water double layer at the platinum surface, but also the platinum-water interaction entirely. Secondly, it entails a much larger simulation which is therefore substantially slower (computer time to perform the simulation is roughly proportional to the square of the number of atoms and hence grows quickly). And finally, it would obscure any effects in the solvent polarization fluctuations that might arise due to the solvent's restriction to the half-space $z > 0$.

There is a way around this problem, however. One can construct a simulation other than the bulk one just described which preserves both the interfacial water interaction, as well as the potential given in Eq. (B5). This can be done by retaining the actual charge q which is fixed a distance d from the interface, and introducing an additional image charge q'' a distance d behind the interface (i.e. at the same position as the earlier $q' = -q$ charge) which is considered as being in vacuum. In other words, one has a solvent with a charge q inside of it, with which it interacts Coloumbically (and perhaps with other forces as well, such as Lennard-Jones, depending on the model). In addition, the solvent interacts with some effective potential that represents a surface at $z = 0$. But there is also an isolated charge q'' a distance d below the $z = 0$ plane, which does not interact with the surface, but does Coloumbically (and only Coloumbically) interact with the solvent. This charge q'' can then be adjusted so that in a continuum model it will give the proper potential which matches with Eq. (B5). Such a simulation, with an isolated charge behind the interface interacting Coloumbically with the solvent, poses no computational difficulties.

If one relies on the superposition of the image and actual charges, the first thing needed is to write down the potential in a continuum model given by the actual charge in the dielectric near another dielectric of constant $\epsilon_2 = 1$ (the vacuum). The earlier Eqs. (B1) and (B2) clearly show that the potential in this case is given by

$$\Phi_a = \frac{q}{\epsilon_1 R} + \frac{1}{\epsilon_1 R'} \frac{\epsilon_1 - 1}{\epsilon_1 + 1} q \quad (B6)$$

Now one can consider the separate and distinct case of the image charge q''' which is located behind the interface in the $z < 0$ region. One wants to find the potential in a continuum model that this charge in vacuum induces in the $z > 0$ region. To do so, one needs to adapt Eqs. (B3) and (B4), originally developed for $z < 0$. The reason for this is that what matters is not really whether z is greater or less than 0, but rather whether one is looking for the potential in the region that contains, or does not contain, the charge of interest. Therefore, in a continuum model, the potential in dielectric 1 due to the charge q''' in vacuum behind the interface is given by

$$\Phi_b = \frac{1}{\epsilon_1 R'} \frac{2\epsilon_1}{1 + \epsilon_1} q''' . \quad (B7)$$

Summing Eqs. (B6) and (B7) and setting the result equal to Eq. (B5), one finds

$$q''' = -q . \quad (B8)$$

Surprisingly the needed charge is simply the negative of the actual charge, independent of the dielectric constant ϵ_1 !

To summarize what has been done : If one is performing a molecular dynamics simulation with a charge q in a solvent a distance d above a conductor, one should add an image charge $-q$ a distance d below the conductor which interacts with the solvent. The purpose of this procedure is to make rigorous contact with the expected results of a dielectric continuum theory. In practice, however, for the simulations detailed in the present work the ion is 5.1 Å from the surface. At such a distance the inclusion of the image charge with the water solvent ($\epsilon \approx 80$) has only a very minor effect.

REFERENCES

- [1] R. A. Marcus and N. Sutin, *Biochimica et Biophysica Acta* **811**, 265 (1985).
- [2] J. Ulstrup, *Charge Transfer Processes in Condensed Media* (Springer, Berlin, 1987)
- [3] E. A. Carter and J. T. Hynes, *J. Phys. Chem.* **93**, 2184 (1989).
- [4] M. Tachiya, *J. Phys. Chem.* **93**, 7050 (1989).
- [5] G. King and A. Warshel, *J. Chem. Phys.* **93**, 8682 (1990); For a review, see A. Warshel and W. W. Parson *Annu. Rev. Phys. Chem.* **42**, 279 (1991)
- [6] T. Kakitani and N. Mataga, *J. Phys. Chem.* **91**, 6277 (1987).
- [7] T. Kakitani and N. Mataga, *J. Phys. Chem.* **90**, 933 (1986).
- [8] R. A. Kuharski, J. S. Bader, D. Chandler, M. Sprik, and R.W. Impey, *J. Chem. Phys.* **89**, 3248 (1988).
- [9] J. S. Bader, R. A. Kuharski, and D. Chandler, *J. Chem. Phys.*, **93**, 230 (1990).
- [10] X. Song and R. A. Marcus, *J. Chem. Phys.* **99**, 7768 (1993).
- [11] J. B. Straus and G. A. Voth, *J. Phys. Chem.* **97**, 7388 (1993).
- [12] I. Benjamin, *J. Phys. Chem.* **95**, 6675 (1991).
- [13] D. A. Rose and I. J. Benjamin, *J. Chem. Phys.* **100**, 3545 (1994).
- [14] P. W. Anderson, *Phys. Rev.* **124**, 41 (1961).
- [15] D. M. Newns, *Phys. Rev.* **178**, 1123 (1969).

[16] T. B. Grimley, in *Progress in Surface and Membrane Science, Vol. 9*, edited by D. A. Cadenhead and J. F. Danielle (Academic, San Francisco, 1975).

[17] J.P. Muscat and D. M. Newns., *Progress in Surface Science* **9**, 1 (1978).

[18] (a) G. A. Voth, D. Chandler, and W. H. Miller, *J. Chem. Phys.*, **91**, 7749 (1989); G. A. Voth, *Chem. Phys. Lett. J. Chem. Phys.*, **170**, 289 (1990); for a review of path integral QTST, see G. A. Voth, *J. Phys. Chem.* **97**, 8365 (1993); (b) see also the related work of M. J. Gillan, *J. Phys. C.* **20**, 3621 (1993).

[19] W. Schmickler, *J. Electroanal. Chem.* **204**, 31 (1986).

[20] K. L. Sebastian, *J. Chem. Phys.* **90**, 5056 (1989).

[21] B. B. Smith and J. T. Hynes, *J. Chem. Phys.* **99**, 6517 (1993).

[22] K. Toukan and A. Rahman, *Phys. Rev. B* **31**, 2643 (1985).

[23] J. Anderson, J. J. Ullo and S. Yip, *J. Chem. Phys.* **87**, 1726 (1987).

[24] S. Nosé, *Mol. Phys.* **52**, 255 (1984).

[25] K. Raghavan, K. Foster, K. Motakabbir, and M. Berkowitz, *J. Chem. Phys.* **94**, 2110 (1991).

[26] E. Spohr and K. Heinzinger, *Ber. Bunsen-Ges. Phys. Chem.* **92**, 1358 (1988).

[27] B. J. Gertner, K. R. Wilson, and J. T. Hynes, *J. Chem. Phys.* **89**, 3537 (1989).

[28] J. Hautman, J.W. Halley, and Y.J. Rhee, *J. Chem. Phys.* **91**, 467 (1989). Note this article contains a typographical error: the units of angstroms for the constants in Eq. 1 of this paper should be omitted.

[29] H.J.C. Berendsen, J.R. Grigera, and T.P. Straatsma, *J. Phys. Chem.* **91**, 6269 (1991).

[30] D. Chandler, *J. Chem. Phys.* **68**, 2959 (1978); J. A. Montgomery, Jr., D. Chandler, and B. J. Berne, *J. Chem. Phys.* **70**, 4056 (1979); R. O. Rosenberg, B. J. Berne, and D. Chandler, *Chem. Phys. Lett.* **75**, 162 (1980); J. Keck, *J. Chem. Phys.* **32**, 1035 (1960); J. B. Anderson, *ibid.* **58**, 4684 (1973); C. H. Bennett, in *ACS Symp. Ser.* **46**, 63 (1977); J. T. Hynes, in *The Theory of Chemical Reactions*, edited by M. Baer (CRC, Boca Raton, FL, 1985); B. J. Berne, in *Multiple Timescales*, edited by J. V. Brackbill and B. I. Cohen (Academic, New York, 1985).

[31] D. Chandler, *Introduction to Modern Statistical Mechanics* (Oxford University Press, 1987).

[32] R. P. Feynman, *Statistical Mechanics*, (Addison Wesley, 1972).

[33] For reviews of path integral methods, both numerical and analytical, see B. J. Berne and D. Thirumalai, *Annu. Rev. Phys. Chem.* **37**, 401 (1986); J. D. Doll, D. L. Freeman and T. L. Beck, *Adv. Chem. Phys.* **78**, 61 (1990); *Quantum Simulations of Condensed Matter Phenomena*, edited by J. D. Doll and J. E. Gubernatis (World Scientific, 1990); D. Chandler, in *Liquides, Cristallisation et Transition Vitreuse, Les Houches, Session LI*, edited by D. Levesque, J. P. Hansen, and J. Zinn-Justin (Elsevier, New York, 1991).

[34] J. H. Lobaugh, Private Communication.

[35] R. A. Kuharski and P. J. Rossky, *J. Chem. Phys.* **82**, 5164 (1985).

[36] J. Cao and G. A. Voth, *J. Chem. Phys.* **100**, 5093 (1994); Cao and G. A. Voth, *ibid* **100**, 5106 (1994);

[37] J. D. Jackson, *Classical Electrodynamics* (John Wiley & Sons, 1975).

FIGURES

FIG. 1. Rectangular periodic cell which permits hexagonal ordering

FIG. 2. Sample two dimensional tiling of space with rectangular periodic cell

FIG. 3. Solid lines gives the diabatic free energy curves for the iron ion 5.1 Å from the Pt surface. The upper solid line is for the Fe^{2+} ion, and the lower solid line is for the Fe^{3+} ion.

FIG. 4. Classical Adiabatic free energy curves for ferrous-ferric charge transfer at the water-Pt(111) interface. Here $\Delta = 0.05$ e.v. Eq. (2.3) was used for the electronic energy contribution, an approximate expression to the electronic portion of the Anderson-Newns Hamiltonian.

FIG. 5. κ vs. time (eq. (2.19)) for ferrous-ferric charge transfer at the water-Pt(111) interface. The final value for κ is 0.5769 ± 0.0004 .

FIG. 6. $\langle r_{OH} \rangle$ vs. P in the monte carlo path integral water simulation of Lobaugh. $P = 25$ was selected as exhibiting converged behavior.

FIG. 7. Adiabatic free energy curve for ferrous-ferric charge transfer at the water-Pt(111) interface using a quantum solvent is shown by the solid line. Eq. (2.3) was used for the electronic energy contribution, an approximate expression to a portion of the Anderson-Newns Hamiltonian. The dashed line shows a best fit to eq. (2.7). The dot-dash line shows the previous classical case.

FIG. 8. $\langle V_{\text{intra}} \rangle$ vs. r_h in molecular dynamics study for $P = 5$.

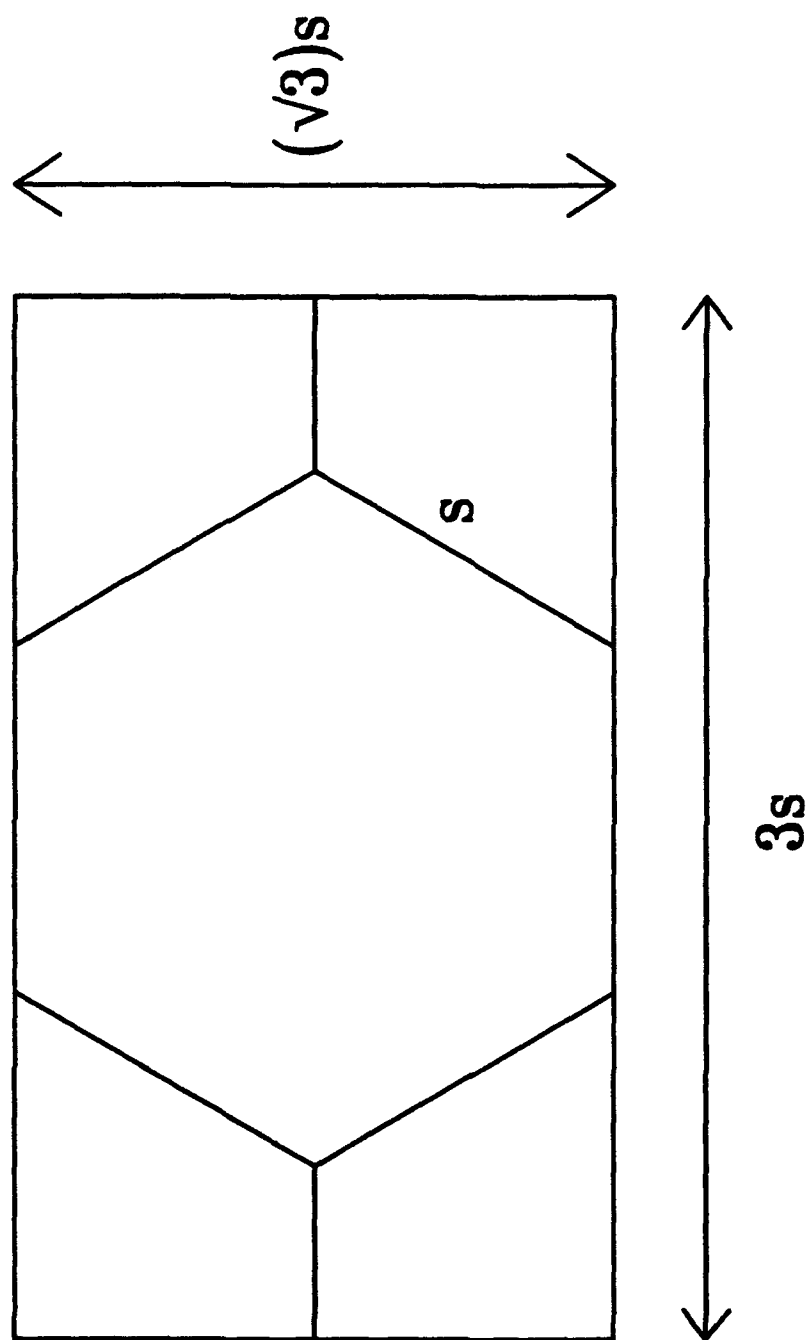
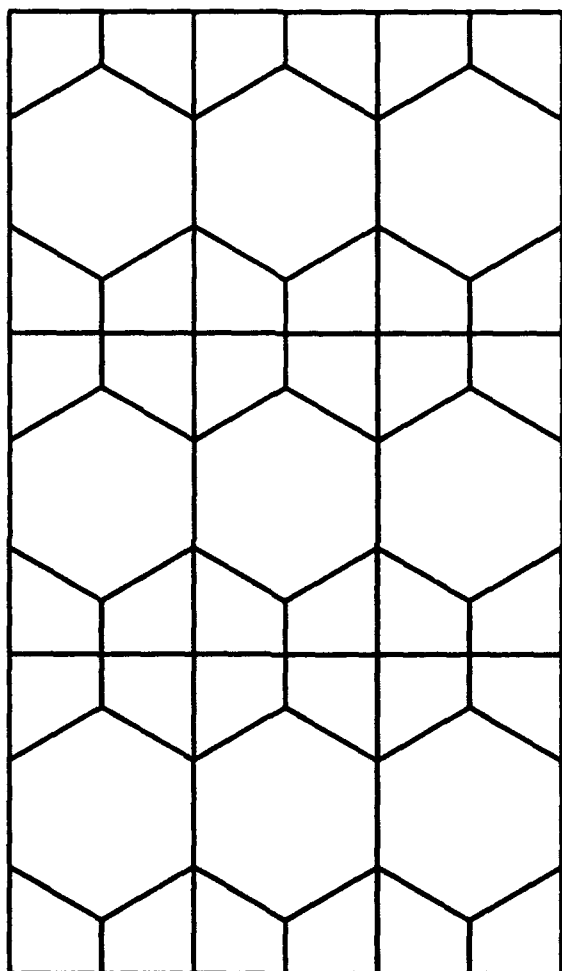


Figure 1

Figure 2



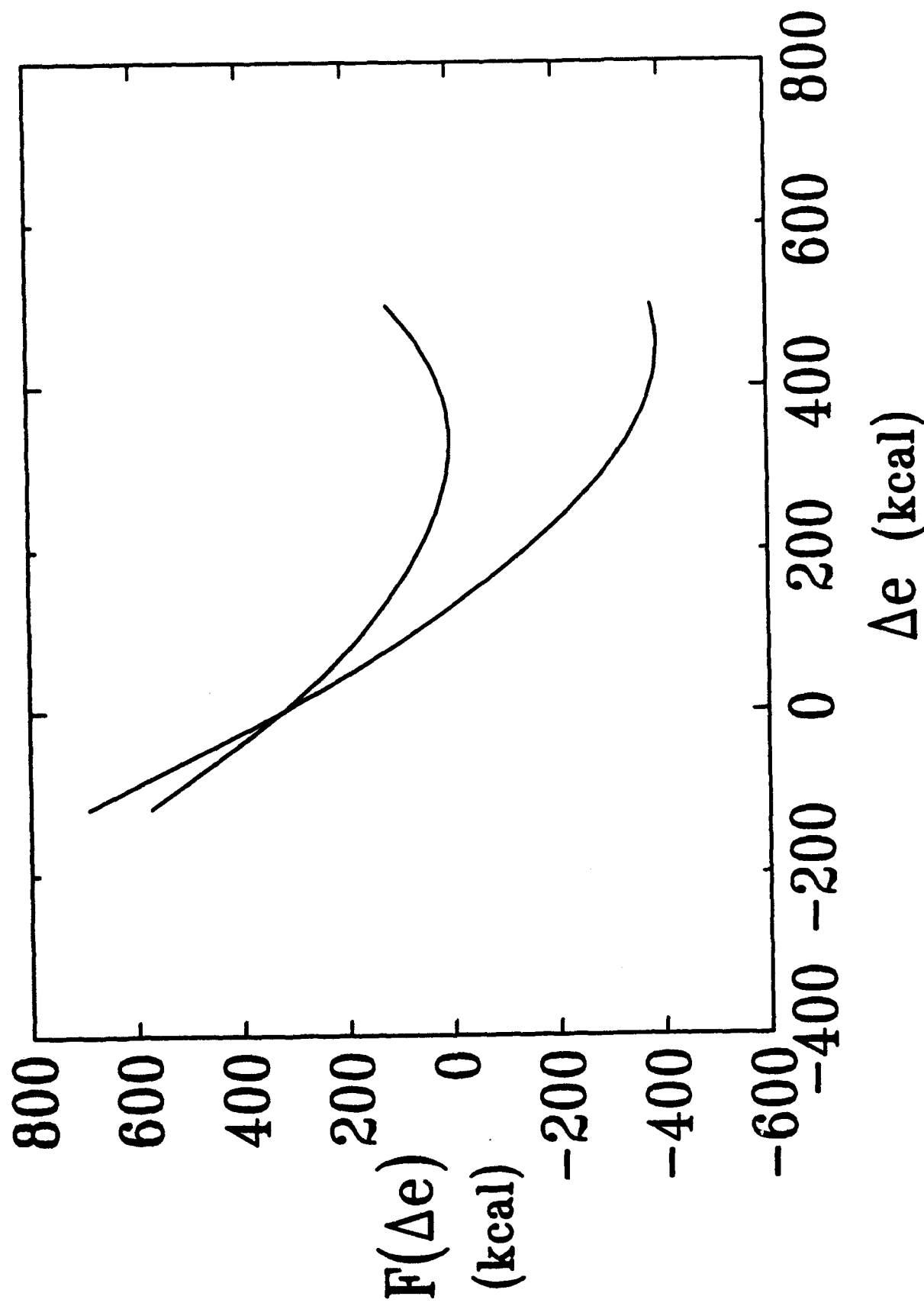


Figure 3

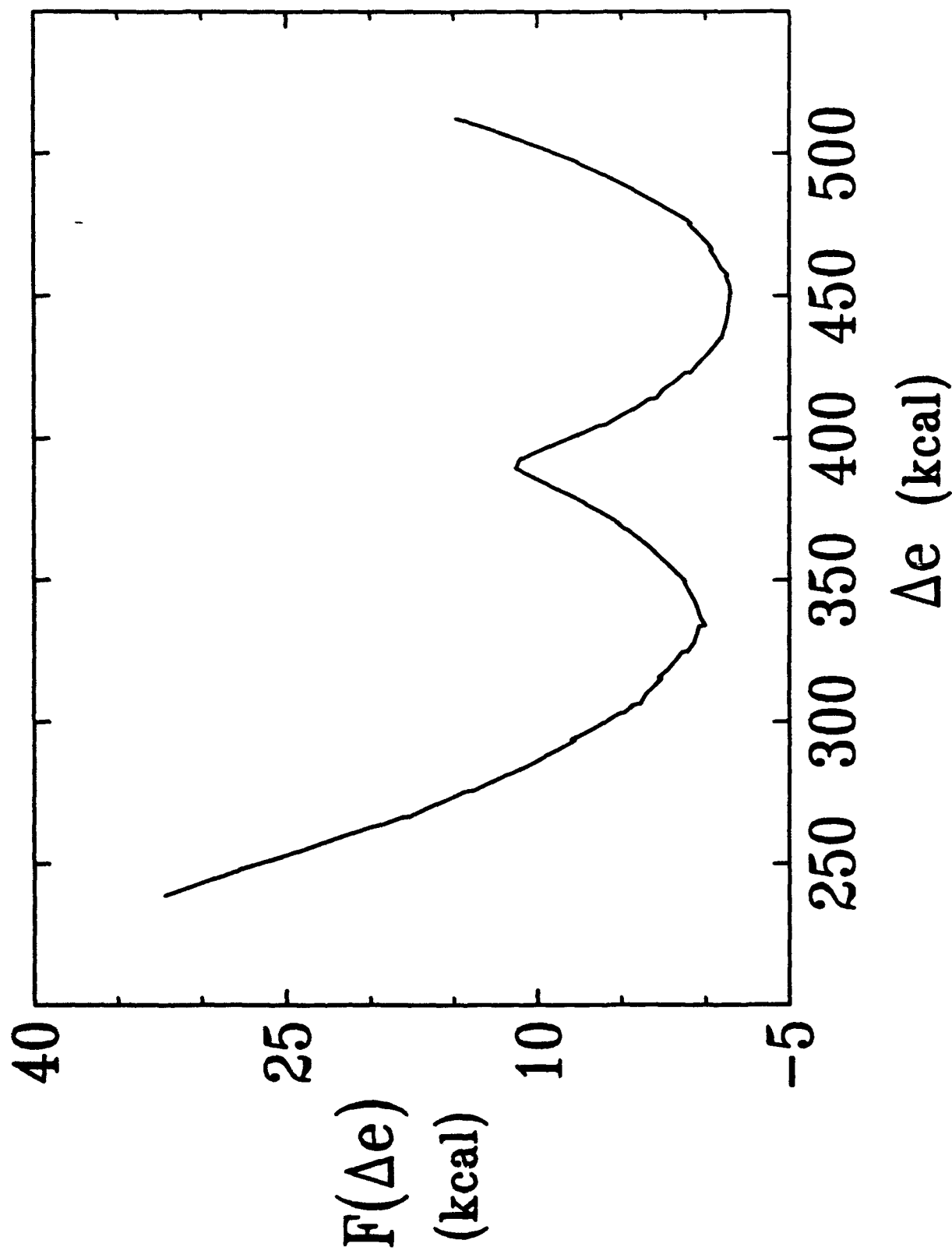


Figure 4

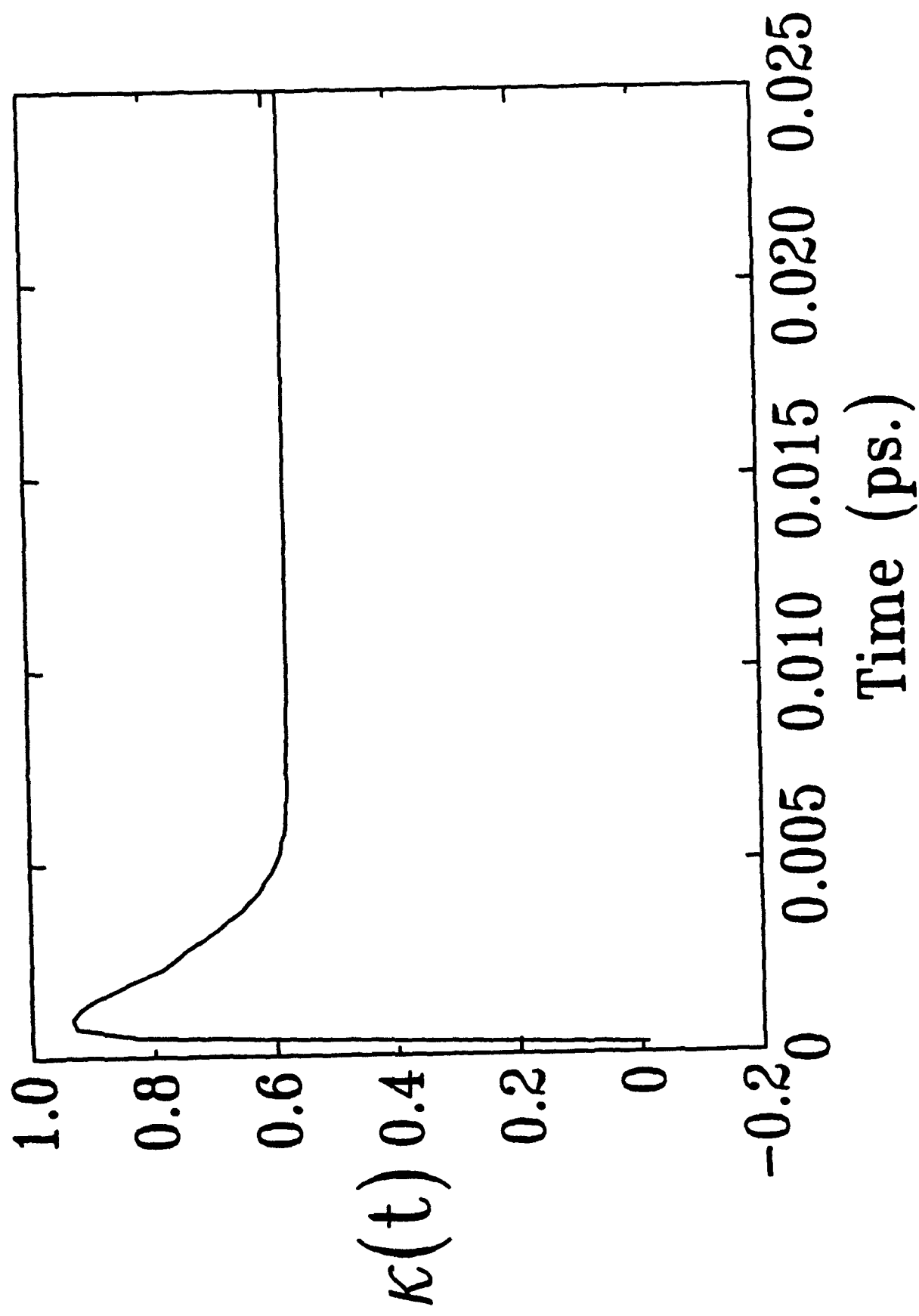


Figure 5

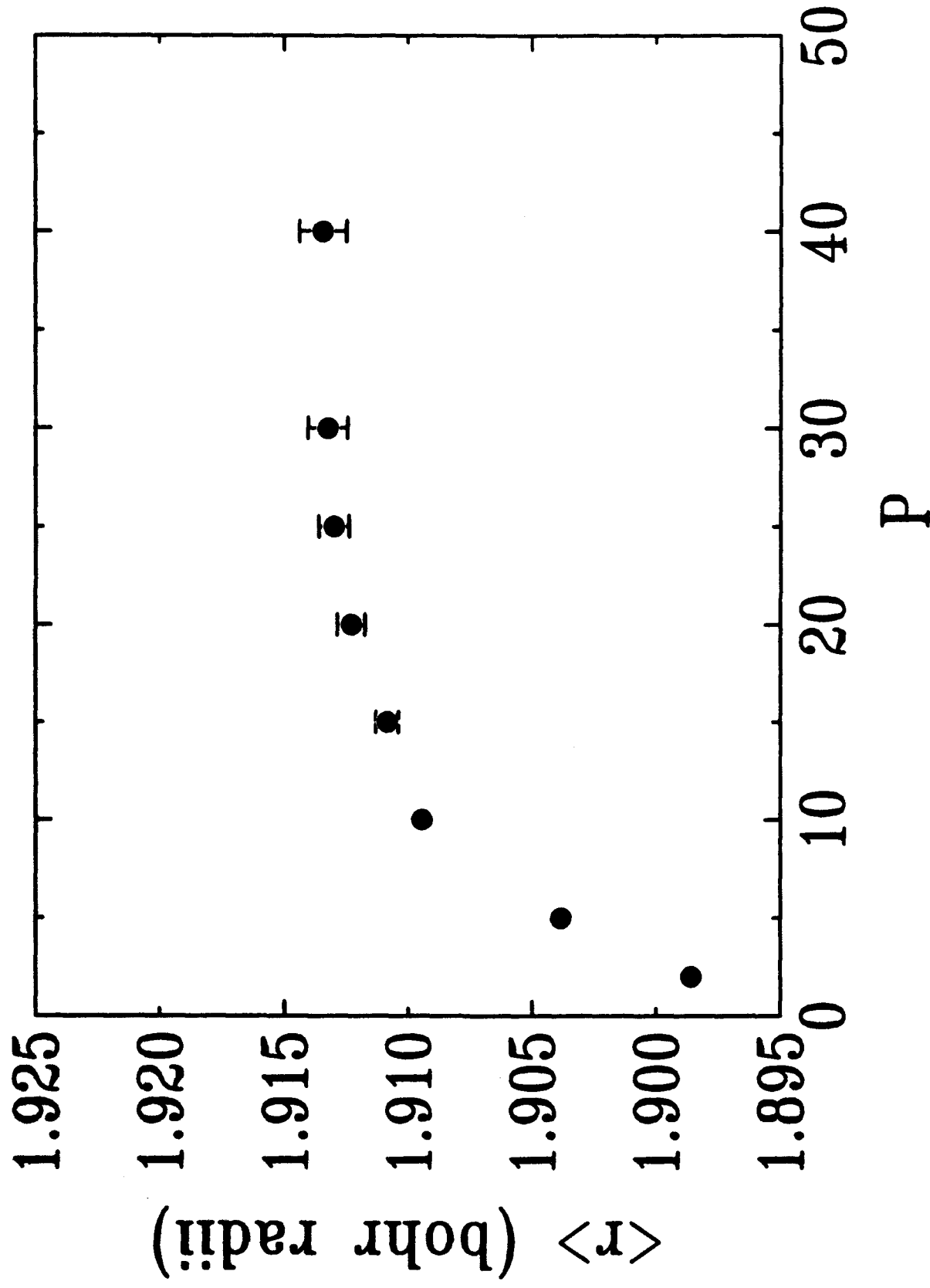


Figure 6

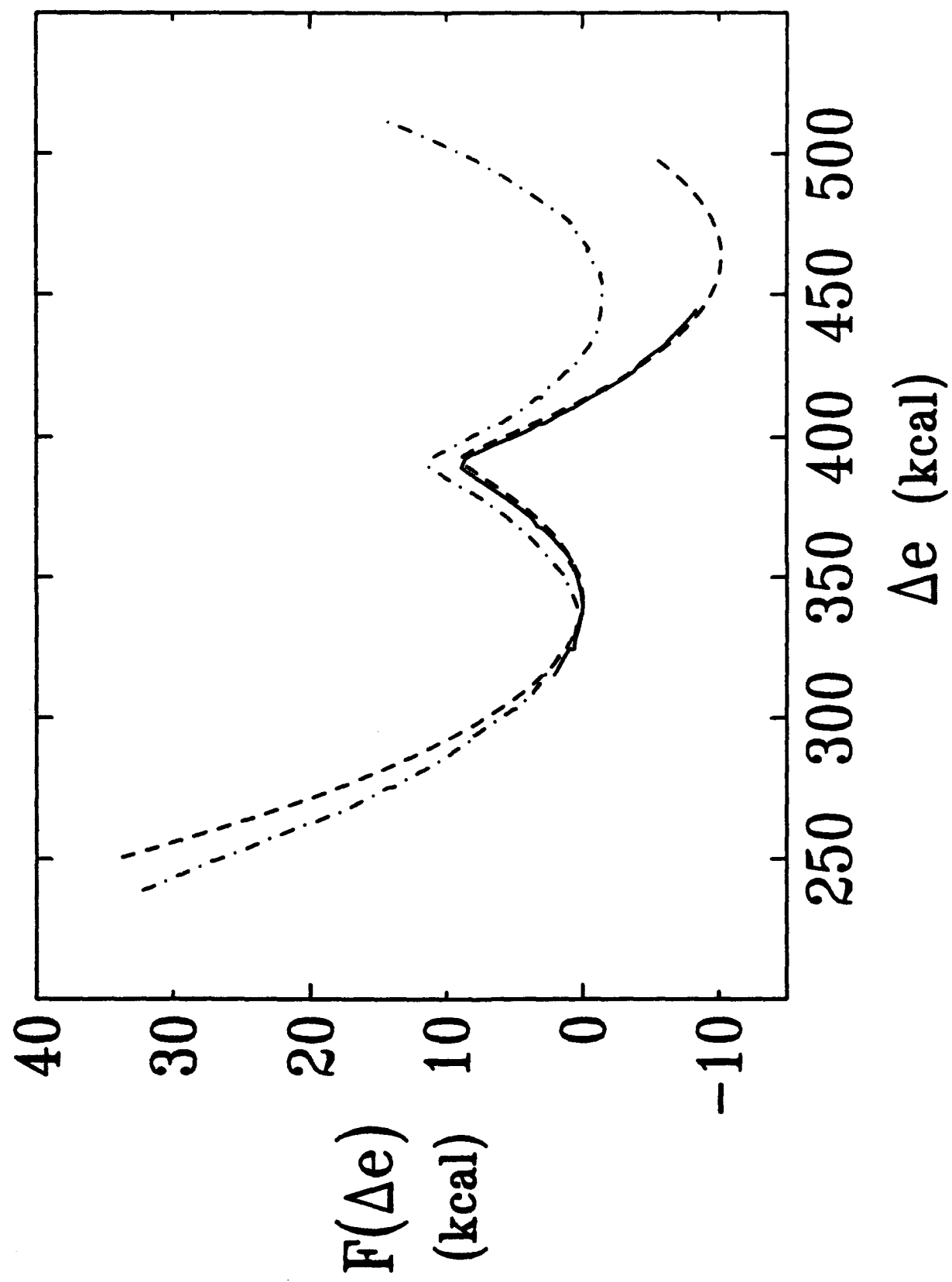


Figure 7

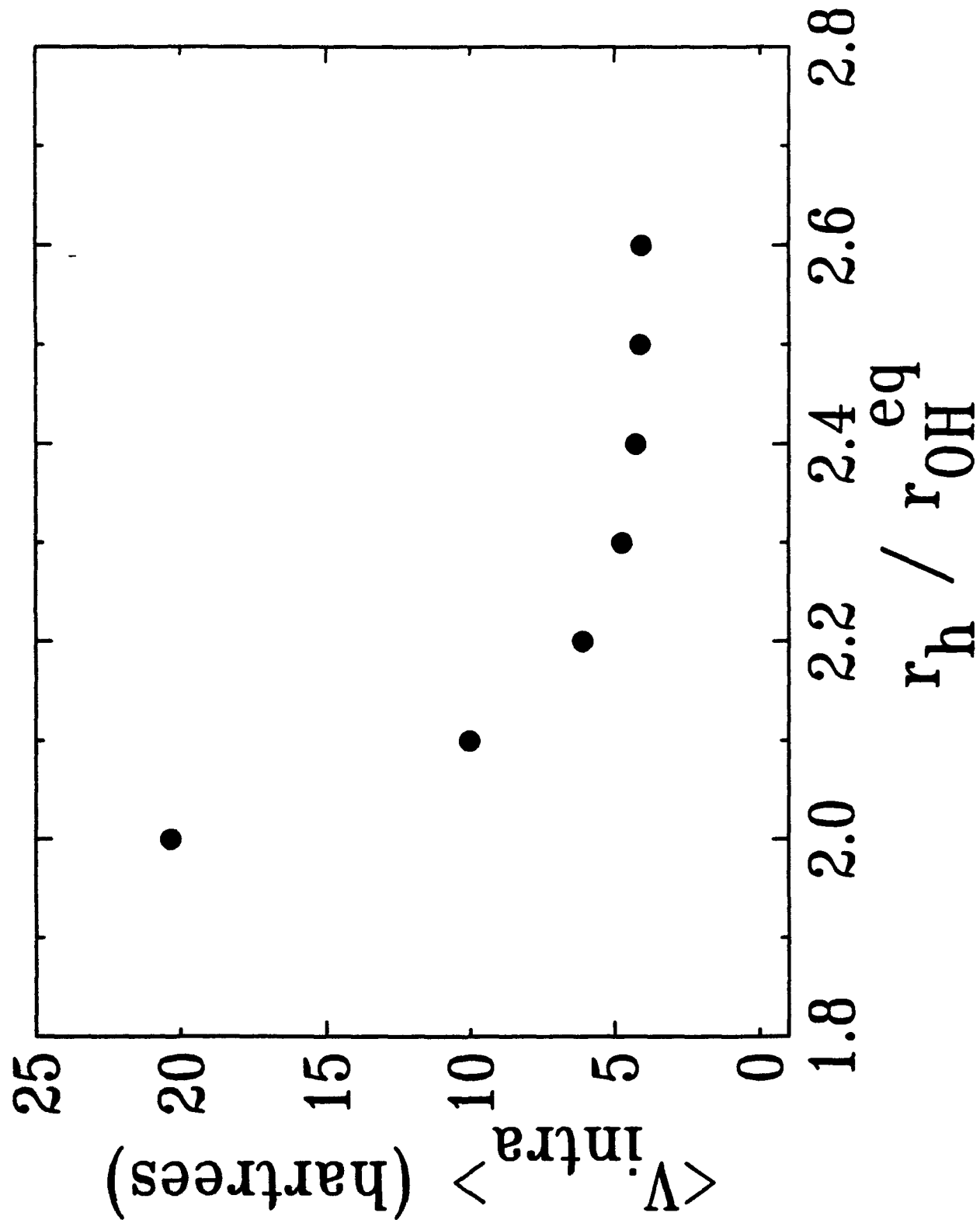


Figure 8